arXiv:1010.5561v2 [nucl-th] 15 Dec 2010

# Shape of $\Lambda$ hypernuclei in $(\beta, \gamma)$ deformation plane

Myaing Thi Win, K. Hagino, and T. Koike
*Department of Physics, Tohoku University, Sendai 980-8578, Japan*

(Dated: December 16, 2010)

We study the shape of $\Lambda$ hypernuclei in the full $(\beta, \gamma)$ deformation plane, including both axially symmetric and triaxial quadrupole deformations. To this end, we use the constrained Skyrme Hartree-Fock+BCS method on the three-dimensional Cartesian mesh. The potential energy surface is analyzed for carbon hypernuclei as well as for sd-shell hypernuclei such as $^{27,29}_{\ \ \Lambda}$Si and $^{25,27}_{\ \ \Lambda}$Mg. We show that the potential energy surface in the $(\beta, \gamma)$ plane is similar to each other between the hypernuclei and the corresponding core nuclei, although the addition of $\Lambda$ hyperon makes the energy surface somewhat softer along the $\gamma$ direction.

PACS numbers: 21.80.+a, 23.20.Lv, 21.30.Fe, 21.60.Jz

## I. INTRODUCTION

One of the main interests in hypernuclear physics is to investigate how an addition of $\Lambda$ particle influences the properties of atomic nuclei. Due to the absence of Pauli's principle between nucleon and $\Lambda$ particle, it is believed that a $\Lambda$ hyperon can be treated as an *impurity* to probe deep interior of the nuclear medium. With the presence of hyperon as an impurity, some bulk properties of nuclei such as the shape and collective motions may be changed [1–3]. Indeed, the shrinkage of $^{7}_{\Lambda}$Li, with respect to $^6$Li, has been observed experimentally by measuring the B(E2) value from the $5/2^+$ state to the $1/2^+$ state of $^{7}_{\Lambda}$Li [4, 5].

As the shape of nuclei plays a decisive role in determining their properties such as quadrupole moment and radius, mean-field model calculations have been performed in recent years to investigate the change of nuclear shape due to the addition of a $\Lambda$ hyperon. Deformed Skyrme-Hartree-Fock(SHF) studies in Ref. [6] have shown that the deformation parameter of the hypernuclei which they studied is slightly smaller (within the same sign) than that of the corresponding core nuclei, and thus no significant effect of $\Lambda$ hyperon on nuclear deformation was found. On the other hand, we have performed a relativistic mean field (RMF) study and found that the nuclear deformation of the core nuclei completely disappears for $^{13}_{\Lambda}$C and $^{29}_{\Lambda}$Si hypernuclei due to the addition of $\Lambda$ particle [7], although we have obtained similar results to the SHF calculations in Ref. [6] for many other hypernuclei. In Ref. [8], we have compared between the SHF and RMF approaches and have shown that the different results with respect to nuclear deformation between the two approaches is due to the fact that the RMF yields a somewhat stronger polarization effect of $\Lambda$ hyperon as compared to the SHF approach. We have also shown that the disappearance of the deformation realizes also in the SHF approach if the energy difference between the optimum deformation and the spherical configuration is less than about 1 MeV [8].

All of these mean-field calculations have assumed axial symmetric deformation. Although many nuclei are considered to have axially symmetric shape, the triaxial degree of freedom plays an important role in transitional nuclei, nuclei with shape coexistence, and nuclei with gamma soft deformation [9–15]. In particular, we mention that recent studies with the constrained Hartree-Fock-Bogoliubov plus local quasi-particle random phase approximation (CHFB+LQRPA) method [16] as well as the RMF plus generator coordinate method (RMF+GCM) [17] have revealed an important role of triaxiality in large amplitude collective motion in sd-shell nuclei.

The aim of this paper is to extend the previous mean-field studies on deformation of hypernuclei by taking into account the triaxial degree of freedom, that is, by including both the $\beta$ and $\gamma$ deformations in order to investigate the effect of $\Lambda$ hyperon in the full $(\beta,\gamma)$ deformation plane. We particularly study the potential energy surface (PES) in $(\beta,\gamma)$ deformation plane with the SHF method for Carbon hypernuclei as well as some sd-shell hypernuclei. Notice that the shape evolution of the C isotopes in the full $(\beta, \gamma)$ plane has been studied by Zhang *et al.* using the SHF method [18]. We extend the work of Zhang *et al.* by introducing a hyperon degree of freedom.

The paper is organised as follows. In Sec. II, we briefly summarise the Skyrme-Hartree-Fock method for hypernuclei. In Sec. III, we present the results for the potential energy surface for the C isotopes as well as for sd-shell nuclei, $^{27,29}_{\ \ \Lambda}$Si and $^{25,27}_{\ \ \Lambda}$Mg. We also discuss the softness of the energy surface along the $\gamma$ deformation. In Sec. IV, we summarize the paper.

## II. SKYRME HARTREE-FOCK+BCS METHOD FOR HYPERNUCLEI

The self-consistent mean field approach provides a useful means to study the ground state properties of hypernuclei. The core polarization effect, that is, the change of properties of a core nucleus due to an addition of $\Lambda$ particle such as a change of total energy and radius can be automatically taken into account with this method [19, 20]. The self-consistent non-relativistic mean field calculations with a Skyrme-type $\Lambda$-nucleon($\Lambda$N) interaction have been performed by Rayet in Refs. [21, 22]. The relativistic mean field approach has also been applied to hypernuclei in *e.g.,* Refs. [23–26]. It has been pointed out that the neutron drip line is extended by the addition of $\Lambda$ hyperon [26, 27].

In the present paper, we employ the Skyrme-type $\Lambda$N interaction and perform mean-field calculations by extending the computer code `ev8` [28] to $\Lambda$ hypernuclei. The code solves the Hartree-Fock equations by discretizing individual single-particle wave functions on a three-dimensional Cartesian mesh. The pairing correlation is taken into account in the BCS approximation. With this method, both axial and triaxial quadrupole deformations can be automatically described. The code `ev8` has been applied to the study of shape transition and deformation of several nuclei [12, 18, 29, 30] in the $(\beta,\gamma)$ deformation plane.

The Skyrme-type $\Lambda$N interaction is given in complete analogy with the nuclear Skyrme interaction [22]. The Skyrme part of the total hypernuclear energy thus reads

$$E = \int d^3r[H_N(\mathbf{r}) + H_\Lambda(\mathbf{r})], \tag{1}$$

where $H_N(\mathbf{r})$ is the standard nuclear Hamiltonian density based on the Skyrme interaction. See *e.g.,* Refs. [31, 32] for its explicit form. $H_\Lambda(\mathbf{r})$ is the hyperon Hamiltonian density given in terms of the lambda and nucleon densities as (with a correction for the coefficient of the $\boldsymbol{\nabla}\rho_N\cdot\boldsymbol{\nabla}\rho_\Lambda$ term) [22]

$$\begin{aligned} H_\Lambda \;=\; & \frac{\hbar^2}{2m_\Lambda}\tau_\Lambda + t_0^\Lambda\left(1+\frac{1}{2}x_0^\Lambda\right)\rho_\Lambda\rho_N \\ & +\frac{1}{4}(t_1^\Lambda + t_2^\Lambda)(\tau_\Lambda\rho_N + \tau_N\rho_\Lambda) \\ & +\frac{1}{8}(3t_1^\Lambda - t_2^\Lambda)(\boldsymbol{\nabla}\rho_N\cdot\boldsymbol{\nabla}\rho_\Lambda) + \frac{1}{4}t_3^\Lambda\rho_\Lambda(\rho_N^2 + 2\rho_n\rho_p) \\ & +\frac{1}{2}W_0^\Lambda(\boldsymbol{\nabla}\rho_N\cdot\boldsymbol{J}_\Lambda + \boldsymbol{\nabla}\rho_\Lambda\cdot\boldsymbol{J}_N). \end{aligned} \tag{2}$$

Here, $\rho_\Lambda$, $\tau_\Lambda$, and $\boldsymbol{J}_\Lambda$ are the particle density, the kinetic energy density, and the spin density of the $\Lambda$ hyperon. These are expressed using the single-particle wave function $\phi_\Lambda$ for the $\Lambda$ particle. $\rho_N$, $\tau_N$, and $\boldsymbol{J}_N$ are the total densities for the nucleons. $t_0^\Lambda, t_1^\Lambda, t_2^\Lambda, t_3^\Lambda, x_0^\Lambda$, and $W_0^\Lambda$ are the Skyrme parameters for the $\Lambda$N interaction.

The Hartree-Fock equations for the single-particle wave functions are obtained by taking variation of the energy $E$. The equation for the nucleons reads,

$$\left[-\boldsymbol{\nabla}\cdot\frac{\hbar^2}{2m_q^*(\boldsymbol{r})}\boldsymbol{\nabla} + V_q(\boldsymbol{r}) + U_N(\boldsymbol{r})\right]\phi_q = e_q\phi_q, \tag{3}$$

where $q$ refers to protons or neutrons, while that for the $\Lambda$ particle reads

$$\left[-\boldsymbol{\nabla}\cdot\frac{\hbar^2}{2m_\Lambda^*(\boldsymbol{r})}\boldsymbol{\nabla} + U_\Lambda(\boldsymbol{r})\right]\phi_\Lambda = e_\Lambda\phi_\Lambda. \tag{4}$$

Here, $e_q$ and $e_\Lambda$ are the single-particle energies and the effective mass for the hyperon is given by

$$\frac{\hbar^2}{2m_\Lambda^*(\boldsymbol{r})} = \frac{\hbar^2}{2m_\Lambda} + \frac{1}{4}(t_1^\Lambda + t_2^\Lambda)\rho_N(\boldsymbol{r}). \tag{5}$$

$V_q(\boldsymbol{r})$ is the single-particle potential originating from the nucleon-nucleon Skyrme interaction [31, 32]. $U_\Lambda(\boldsymbol{r})$ and $U_N(\boldsymbol{r})$ are the single-particle potentials originating from the $\Lambda$N interaction. These are expressed as [22]

$$\begin{aligned} U_\Lambda(\boldsymbol{r}) \;=\; & t_0^\Lambda\left(1+\frac{1}{2}x_0^\Lambda\right)\rho_N + \frac{1}{4}\left(t_1^\Lambda + t_2^\Lambda\right)\tau_N \\ & -\frac{1}{8}\left(3t_1^\Lambda - t_2^\Lambda\right)\nabla^2\rho_N + \frac{t_3^\Lambda}{4}\left(\rho_N^2 + 2\rho_n\rho_p\right) \\ & -\frac{1}{2}W_0^\Lambda\boldsymbol{\nabla}\cdot\boldsymbol{J}_N \\ & +\frac{1}{2}W_0^\Lambda\boldsymbol{\nabla}\rho_N\cdot(-i\boldsymbol{\nabla}\times\boldsymbol{\sigma}), \end{aligned} \tag{6}$$

and

$$\begin{aligned} U_N(\boldsymbol{r}) \;=\; & t_0^\Lambda\left(1+\frac{1}{2}x_0^\Lambda\right)\rho_\Lambda + \frac{1}{4}\left(t_1^\Lambda + t_2^\Lambda\right)\tau_\Lambda \\ & -\frac{1}{8}\left(3t_1^\Lambda - t_2^\Lambda\right)\nabla^2\rho_\Lambda \\ & +\frac{t_3^\Lambda}{4}\rho_\Lambda(2\rho_N + 2(\rho_N - \rho_q)) - \frac{1}{2}W_0^\Lambda\boldsymbol{\nabla}\cdot\boldsymbol{J}_\Lambda \\ & +\frac{1}{2}W_0^\Lambda\boldsymbol{\nabla}\rho_\Lambda\cdot(-i\boldsymbol{\nabla}\times\boldsymbol{\sigma}). \end{aligned} \tag{7}$$

The pairing correlations among the nucleons are treated in the BCS approximation. For the pairing interaction, we employ a zero-range density-dependent pairing force [33],

$$V(\mathbf{r_1},\mathbf{r_2}) = -g\,\frac{1-\hat{P}^\sigma}{2}\left(1-\frac{\rho(\bar{\boldsymbol{r}})}{\rho_0}\right)\delta(\boldsymbol{r}_1 - \boldsymbol{r}_2), \tag{8}$$

where $\hat{P}^\sigma$ is the spin-exchange operator, $\rho_0 = 0.16$ fm$^{-3}$, and $\bar{\boldsymbol{r}} = (\boldsymbol{r}_1 + \boldsymbol{r}_2)/2$.

In this paper, we mainly use the SGII interaction [34] for the NN interaction, while the set No.1 in Ref. [35] for the $\Lambda$N interaction. The latter interaction was constructed by fitting to the binding energy of $^{17}_{\Lambda}$O, yielding the well depth for a $\Lambda$ particle, $D_\Lambda$= 29.38 MeV, in infinite nuclear matter. Notice that the spin-orbit strength $W_0^\Lambda$ in the $\Lambda N$ interaction is zero for the set No. 1 [35]. For the pairing interaction, we follow Ref. [18] to use $g = 410$ MeV·fm$^3$ for both protons and neutrons for Carbon hypernuclei, while we follow Ref. [33] to use $g = 1000$ MeV·fm$^3$ for calculations of sd-shell hypernuclei. A smooth pairing energy cutoff of 5 MeV around the Fermi level is used [33]. We assume that the $\Lambda$ particle occupies the lowest single-particle state.

Since the primary purpose of this paper is to draw the potential energy surfaces (PES) of $\Lambda$ hypernuclei as a function of $\beta$ and $\gamma$ deformation parameters, the isoscalar quadrupole constraint is imposed on the total energy. We relate the deformation parameter $\beta$ for hypernuclei with the total quadrupole moment $Q$ using the equation

$$\beta \approx \frac{\sqrt{5\pi}Q}{3(A_c+1)R_0^2}, \tag{9}$$

where $A_c = A-1$ is the mass number of the core nucleus and $R_0 = 1.2A_c^{1/3}$ fm is the radius of the hypernucleus.

## III. RESULTS

### A. Carbon Hypernuclei

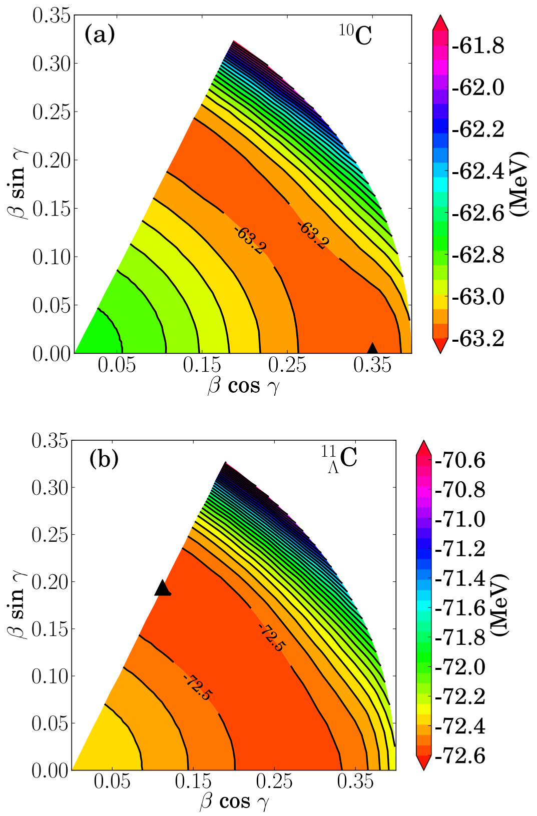

FIG. 1: (Color online) The potential energy surface (PES) of (a) $^{10}$C and (b) $^{11}_{\Lambda}$C in the $(\beta, \gamma)$ deformation plane obtained with the SGII parameter set. Each contour line is separated by 0.07MeV. The triangles indicate the absolute minima in the PES.

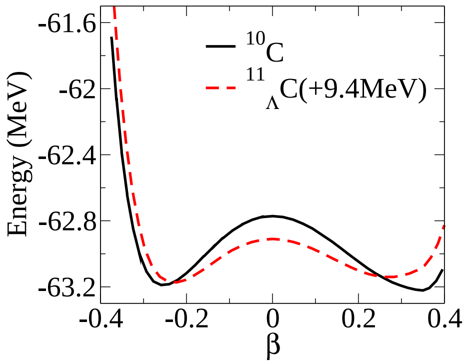

FIG. 2: The energy curve for $^{10}$C and $^{11}_{\Lambda}$C along the axially symmetric deformation corresponding to Fig. 1. The energy surface for $^{11}_{\Lambda}$C is shifted by a constant amount as indicated in the figure.

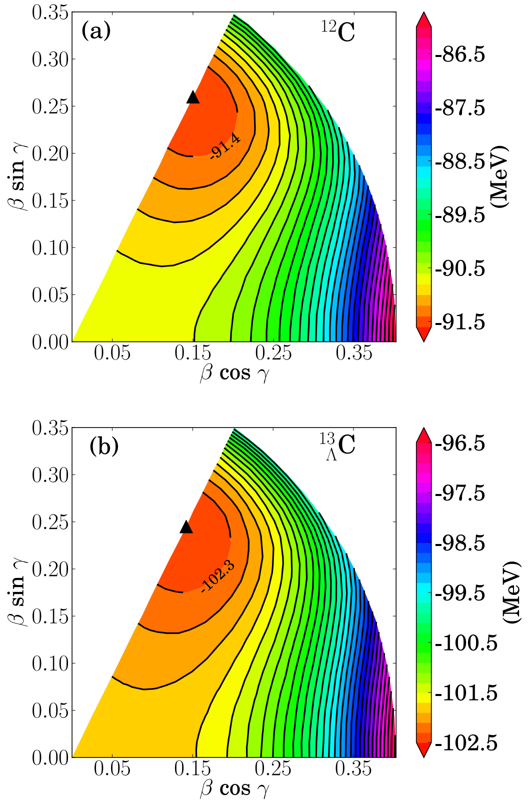

FIG. 3: (Color online) Same as Fig. 1, but for $^{12}$C and $^{13}_{\Lambda}$C. Each contour line is separated by 0.2MeV.

We now numerically solve the Hartree-Fock equations and discuss the deformation properties of hypernuclei in the $(\beta, \gamma)$ deformation plane. We first investigate the shape of carbon hypernuclei from $^{11}_{\Lambda}$C to $^{23}_{\Lambda}$C. To this end, we follow Refs. [6, 8, 18, 36] and reduce the strength of the spin-orbit interaction by a factor of 0.6 in the Skyrme functional. This prescription was introduced in order to reproduce an oblate ground state of $^{12}$C [36].

Figure 1 shows the potential energy surfaces for $^{10}$C and $^{11}_{\Lambda}$C so obtained. The triangles in the figure indicate the ground state minimum in the energy surface. The energy curve along the axially symmetric deformation is also shown in Fig. 2 as a function of the quadrupole deformation parameter $\beta$. Along the axially symmetric configuration, there are deep energy minima in both sides of prolate and oblate configurations of $^{10}$C (that is, the shape coexistence), having a very small energy difference of less than 40 keV between them. The ground state corresponds to the prolate configuration with $\beta$=0.35. However, the energy surface is almost flat along the triaxial deformation $\gamma$ as one can see in Fig. 1 (a) in the $(\beta, \gamma)$ deformation plane. With the addition of a $\Lambda$ hyperon, the ground state configuration moves from prolate to oblate, although the energy surface is so flat along the $\gamma$ degree of freedom (see Fig. 1(b)) that the ground state configuration may not be well defined in the mean field

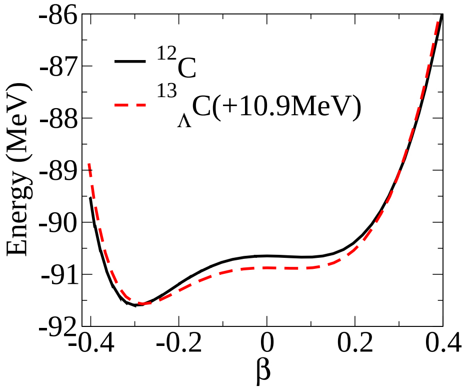

FIG. 4: (Color online) Same as Fig.2, but for $^{12}$C and $^{13}_{\Lambda}$C.

approximation. We have confirmed that this feature remains the same even if we use the Skyrme ΛN interaction set No.2 and No. 5 [35], instead of No. 1.

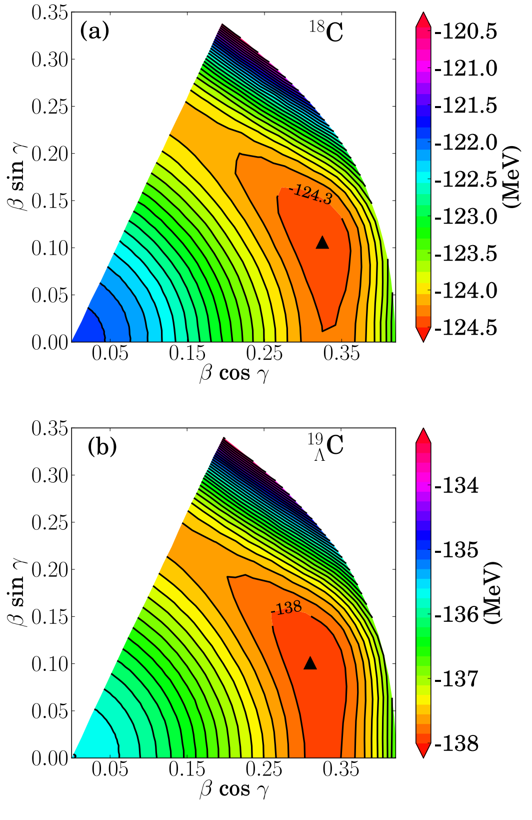

FIG. 5: (Color online) Same as Fig. 1, but for $^{18}$C and $^{19}_{\Lambda}$C. Each contour line is separated by 0.15MeV

Figs. 3 (a) and 4 show the energy surface for $^{12}$C in the $(\beta, \gamma)$ deformation plane and that along the $(\beta, \gamma = 0)$ line, respectively. For this nucleus, the Skyrme-Hartree-Fock method with the reduced spin-orbit interaction yields a deep oblate minimum. In this case, the addition of a Λ particle shows little effect on the energy surface, although the deformation is slightly smaller than its core nucleus (see Figs. 3(b) and 4). This is similar to the result for $^{20}$Ne discussed in Ref.[7] with the RMF method.

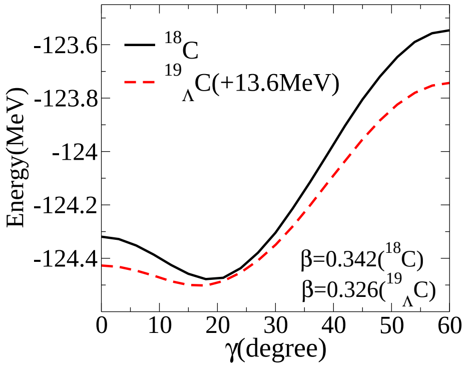

FIG. 6: (Color online) The energy curve as a function of the triaxial deformation parameter $\gamma$ for the optimum values of the $\beta$ deformation parameters shown in Fig. 5. The energy surface for $^{19}_{\Lambda}$C is shifted by a constant amount as indicated in the figure.

For the case of $^{18}$C, it has a triaxial minimum at $\beta = 0.34$ and $\gamma = 18.0°$ at an energy of $-0.154$MeV with respect to the prolate configuration (see Fig. 5 (a)). We find that $^{19}_{\Lambda}$C has a ground state configuration with similar values of $\beta$ and $\gamma$ deformation parameters to those of the core nucleus, $^{18}$C, as indicated in Fig. 5 (b). The triaxial minimum is again shallow with an energy difference of 0.077 MeV between the optimum deformation and the prolate configuration. In Fig. 6, we plot the energy curve as a function of the triaxial deformation parameter $\gamma$ for the optimum values of the $\beta$ deformation parameter. With the addition of a Λ particle to $^{18}$C, one sees that the energy curve becomes slightly softer (compare also Figs. 5(a) and 5(b)).

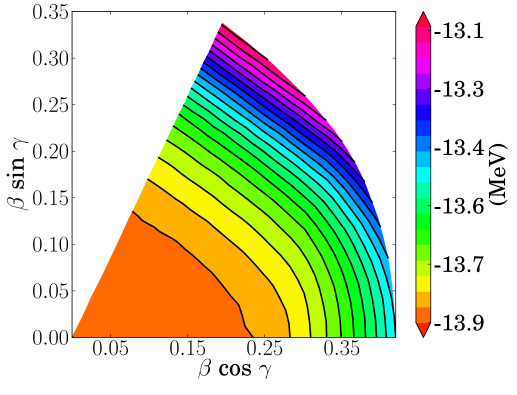

FIG. 7: (Color online) The energy difference between $^{19}_{\Lambda}$C and $^{18}$C nuclei in the $(\beta, \gamma)$ deformation plane.

The energy difference between $^{19}_{\Lambda}$C and $^{18}$C at each deformation, that is, $E_{^{19}_{\Lambda}\mathrm{C}}(\beta, \gamma) - E_{^{18}\mathrm{C}}(\beta, \gamma)$, in the $(\beta, \gamma)$ deformation plane is plotted in Fig. 7. It clearly shows that the addition of a $\Lambda$ particle prefers the spherical configuration even if the core nucleus has a deformed minimum. We have confirmed that this is the case for the other carbon isotopes as well. Notice that the $\Lambda$ particle slightly prefers the prolate configuration for a fixed value of $\beta$, causing the slightly softer energy curve towards the prolate configuration shown in Fig. 5. This originates from the fact that the overlap between the deformed nuclear density and a spherical $\Lambda$ density is maximum at the prolate configuration, as we discuss in the Appendix.

The results of our calculations are summarised in Table I, together with the results for the other carbon isotopes.

## B. sd shell Hypernuclei

### 1. *Potential Energy Surface*

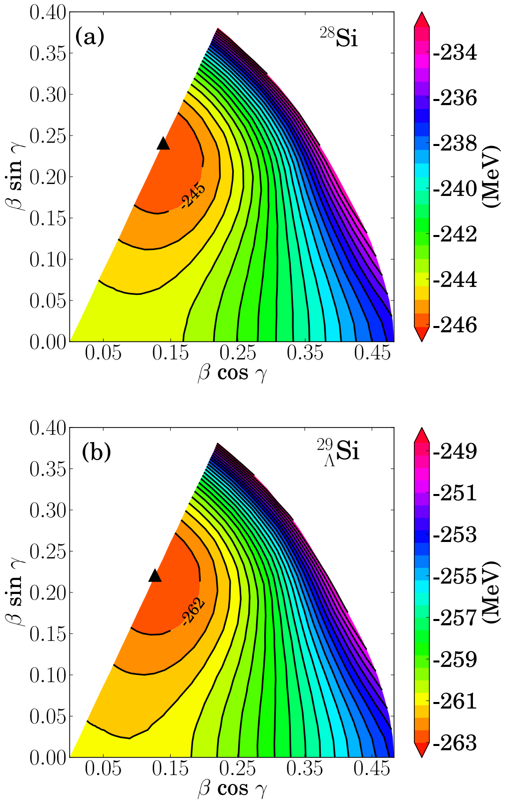

FIG. 8: (Color online) Same as Fig. 1, but for $^{28}$Si and $^{29}_{\Lambda}$Si. Each contour line is separated by 0.6 MeV.

Let us next discuss the deformation energy surfaces of $^{27,29}_{\Lambda}$Si,and $^{25,27}_{\Lambda}$Mg nuclei in the $(\beta,\gamma)$ deformation plane. For these nuclei, we use the original strength for the spin-orbit interaction. We first show the potential energy surface of $^{28}$Si and $^{24}$Mg in Figs. 8(a) and Fig. 9(a), respectively. The energy surface for $^{28}$Si shows a deep oblate minimum, while that for $^{24}$Mg shows a deep prolate minimum. Notice that N=Z=14 is an oblate magic number. The energy curves for $^{24}$Mg as a function of $\beta$ with $\gamma = 0$, and of $\gamma$ with $\beta = \beta_{\rm min} = 0.387$ are also plotted in in Figs. 10(a) and 10(b), respectively.

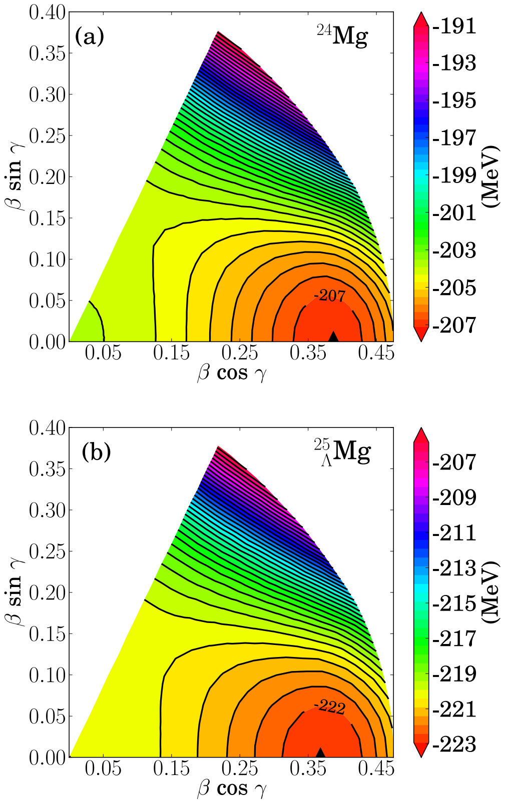

FIG. 9: (Color online) Same as Fig. 1, but for $^{24}$Mg and $^{25}_{\Lambda}$Mg. Each contour line is separated by 0.5 MeV.

For these nuclei, as the potential minimum is deep, the addition of a $\Lambda$ particle does not change significantly the shape of the potential energy surface, as shown in Figs. 8(b), 9(b),and 10. As shown in the previous subsection, the energy gain due to the additional $\Lambda$ particle appears mainly around the spherical configuration. Notice, however, that the $\Lambda$ particle makes the energy curve slightly softer along the triaxial degree of freedom, $\gamma$.

We next discuss the $^{27}_{\Lambda}$Mg and $^{27}_{\Lambda}$Si nuclei. $^{26}$Mg has Z=12 and N=14, that is, the protons favour a prolate configuration while the neutrons favour an oblate configuration. As a competition of these two opposite effects, the structure of $^{26}$Mg may not be trivial [16]. $^{26}$Si is the mirror nucleus of $^{26}$Mg, and the deformation properties are expected to be similar to $^{26}$Mg.

Figures 11(a) and Fig. 12(a) show the potential energy surfaces for $^{26}$Si and $^{26}$Mg, respectively. Indeed, the two energy surfaces are similar to each other, and show an oblate minimum with a considerably flat surface along the $\gamma$ direction. The energy difference between the oblate and the prolate configurations is 0.12 MeV for $^{26}$Si and

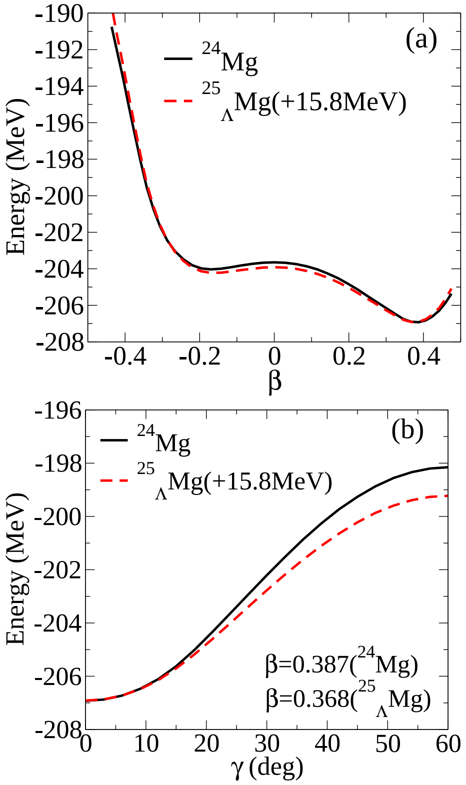

FIG. 10: (Color online) (a) The energy curve for $^{24}$Mg and $^{25}_{\Lambda}$Mg along the axially symmetric deformation corresponding to Fig. 9. (b) The energy curve as a function of the triaxial deformation parameter $\gamma$ for the optimum values of the $\beta$ deformation parameters shown in Fig. 9. The energy surfaces for $^{25}_{\Lambda}$Mg are shifted by a constant amount as indicated in the figures.

0.39 MeV for $^{26}$Mg. The energy curve for $^{26}$Mg as a function of $\beta$ with $\gamma = 0$, and of $\gamma$ with $\beta = \beta_{\rm min} = 0.226$ are plotted in in Figs. 13(a) and 13(b), respectively. The energy curves for $^{26}$Si are qualitatively similar, and are not shown.

As in $^{24}$Mg and $^{28}$Si, the addition of a $\Lambda$ hyperon does not significantly alter the potential energy surface of these nuclei, although it somewhat softens the energy surface along the $\gamma$ direction (see Figs. 11(b), 12(b), and 13). We again find that the additional $\Lambda$ particle favours the spherical configuration.

The calculations presented in this subsection are performed with the SGII set of the Skyrme interaction. We have repeated the same calculations with another Skyrme parameter, SIII, and have found that the results are qualitatively the same as the results obtained with SGII.

### 2. *γ vibration*

For a long time, the $^{24}$Mg nucleus has been considered to be a candidate of nuclei with a triaxial shape, because of the low-lying second $2^+$state in the rotational spectrum [37]. That is, the experimental spectrum of $^{24}$Mg has been interpreted as consisting of a $K$=0 ground state rotational band and a $K$=2 rotational band built upon a $\gamma$ vibrational state at 4.23 MeV [38, 39]. The previous mean-field calculations for the ground state of $^{24}$Mg using RMF [40] and SHF [41] have shown an axially symmetric prolate ground state. Recently, it has been pointed out that the angular momentum projection is essential in order to reproduce the triaxial ground state of $^{24}$Mg[42]. The 3-dimensional angular momentum projection plus generator coordinate method (3DAMP+GCM) calculations have shown a good agreement with the experimental data on low-spin states of $^{24}$Mg [42].

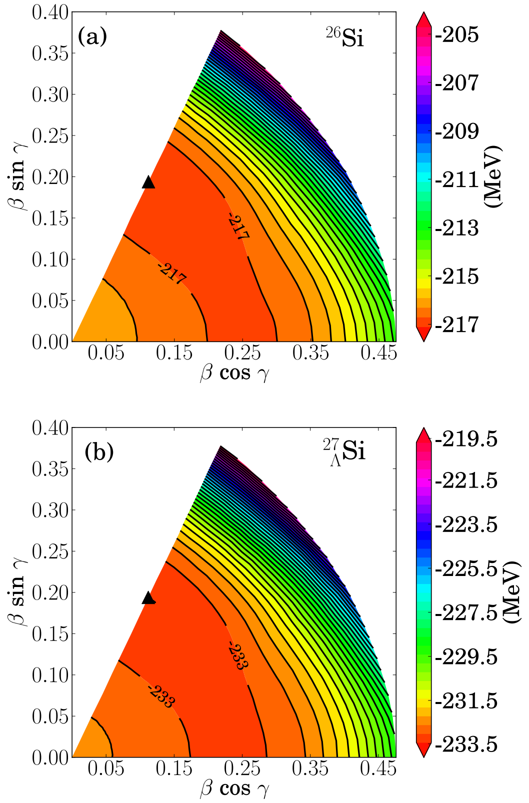

FIG. 11: (Color online) Same as Fig. 1, but for $^{26}$Si and $^{27}_{\Lambda}$Si. Each contour line is separated by 0.4 MeV.

In order to see the effect of $\Lambda$ hyperon on $\gamma$ vibration, we compute the second derivative of the energy curve with respect to $\gamma$ around the minimum, $(\beta_0, \gamma_0)$. That is, when we approximate the energy curve around the minimum as,

$$E(\beta_0, \gamma) \approx E(\beta_0, \gamma_0) + \frac{1}{2} D\omega^2 \gamma^2, \qquad (10)$$

the second derivative $E''$ provides information on the frequency $\omega$ for the $\gamma$ vibration if the vibrational moment of inertia $D$ is known. By numerically taking the

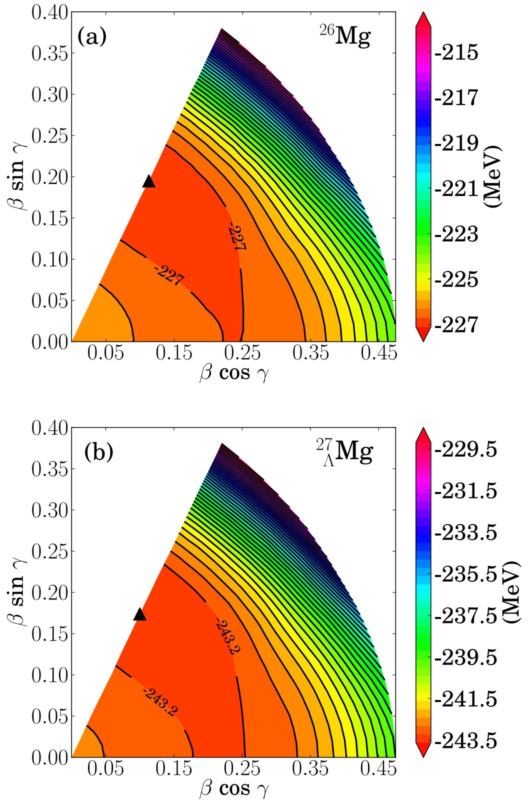

FIG. 12: (Color online) Same as Fig. 1, but for $^{26}$Mg and $^{27}_{\Lambda}$Mg. Each contour line is separated by 0.4 MeV.

second derivative, we obtain $E''_{^{25}_{\Lambda}Mg}/E''_{^{24}Mg} = 0.961$ and $E''_{^{27}_{\Lambda}Mg}/E''_{^{26}Mg} = 0.988$. That is, the addition of a $\Lambda$ particle makes the $\gamma$ vibration softer if the change in the moment of inertia $D$ is negligible.

Although the $\Lambda$ particle softens the energy curve both for $^{25}_{\Lambda}$Mg and $^{27}_{\Lambda}$Mg, the mechanism is somewhat different between the two nuclei. For the $^{27}_{\Lambda}$Mg nucleus, the prolate configuration decreases more energy as compared to the oblate configuration (see Fig. 13 (b)), because the prolate configuration has a larger overlap between the $\Lambda$ particle and the nucleon densities, as is discussed in the Appendix. As a consequence, the curvature of the energy curve at the oblate minimum becomes smaller with the addition of a $\Lambda$ particle. In contrast, the effect of the smaller value of $\beta$ is more significant in $^{25}_{\Lambda}$Mg. That is, the energy curve along the axially symmetric configuration is considerably steep for $\beta \leq -0.2$ (see Fig. 10 (a)), and even a small change in $\beta$ induces a significant energy change at the oblate configuration. Therefore, for $^{25}_{\Lambda}$Mg, the energy decreases more at the oblate side as compared to the prolate side for a fixed value of $\beta$ (see Fig. 10 (b)), leading to the softer gamma-vibration. Notice that the absolute value of $\beta$ is relatviely small for $^{26}$Mg, lying in a "flat" region, and this effect is much less important in the $^{27}_{\Lambda}$Mg nucleus.

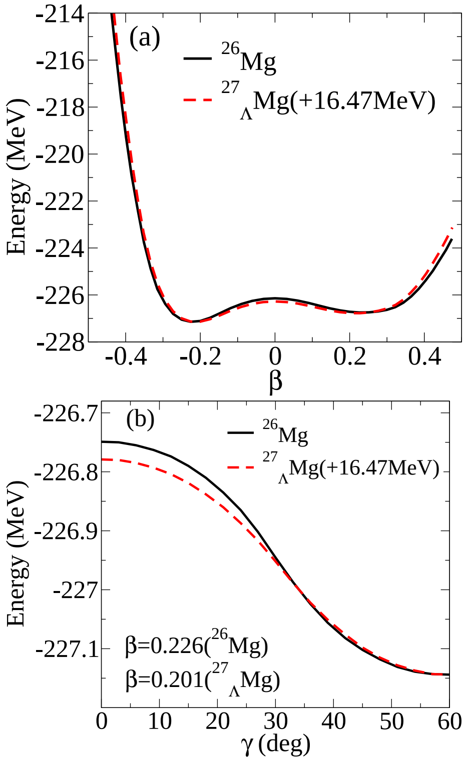

FIG. 13: (Color online) (a) The energy curve for $^{26}$Mg and $^{27}_{\Lambda}$Mg along the axially symmetric deformation corresponding to Fig. 12. (b) The energy curve as a function of the triaxial deformation parameter $\gamma$ for the optimum values of the $\beta$ deformation parameters shown in Fig. 12. The energy surfaces for $^{27}_{\Lambda}$Mg are shifted by a constant amount as indicated in the figures.

## IV. SUMMARY

We have investigated the shape of $\Lambda$ hypernuclei in the $(\beta,\gamma)$ deformation plane with the Skyrme-Hartree-Fock + BCS approach. In contrast to the previous mean-field studies, we have taken into account the triaxial deformation using a 3-D Cartesian mesh method. We have studied the potential energy surface for the Carbon hypernuclei from $^{11}_{\Lambda}$C to $^{23}_{\Lambda}$C as well as sd-shell hypernuclei $^{27}_{\Lambda}$Si, $^{29}_{\Lambda}$Si, $^{25}_{\Lambda}$Mg and $^{27}_{\Lambda}$Mg. The potential energy surface for $^{10}$C, $^{26}$Mg, and $^{26}$Si is characterized by a flat surface along the $\gamma$ degree of freedom connecting the prolate and the oblate configurations. We have found that the addition of a $\Lambda$ particle makes the energy surface slightly softer along the triaxial degree of freedom, although the gross feature of the energy surface remains similar to the energy surface for the corresponding core nuclei.

In Refs. [7, 8], we have argued that the influence of the addition of a $\Lambda$ particle is stronger in the relativistic mean-field approach as compared to the non-relativistic Skyrme-Hartree-Fock approach employed in this paper. This implies that the softening of the energy curve for the $\gamma$-vibration may be larger than that estimated in this pa-

TABLE I: The quadrupole deformation parameters $\beta$ and $\gamma$ (in deg.), and the ground state energy obtained with the Skyrme interaction SGII parameter set. $\beta_p$, $\beta_n$, $\beta_\Lambda$, and $\beta_{\rm tot}$ ($\gamma_p$, $\gamma_n$, $\gamma_\Lambda$, and $\gamma_{\rm tot}$) are the deformation parameters for proton, neutron, $\Lambda$ particle, and the whole nucleus, respectively.

| nucleus | $\beta_p$ | $\beta_n$ | $\beta_\Lambda$ | $\beta_{\rm tot}$ | $\gamma_p$ | $\gamma_n$ | $\gamma_\Lambda$ | $\gamma_{\rm tot}$ | $-E$ (MeV) |
|---|---|---|---|---|---|---|---|---|---|
| $^{10}$C | 0.182 | 0.175 | - | 0.35 | 0 | 0 | - | 0 | 63.222 |
| $^{11}_{\Lambda}$C | 0.140 | 0.087 | 0.010 | 0.223 | 59.619 | 60 | 59.723 | 59.989 | 72.573 |
| $^{12}$C | 0.154 | 0.151 | - | 0.301 | 60 | 59.969 | - | 60 | 91.6 |
| $^{13}_{\Lambda}$C | 0.145 | 0.142 | 0.012 | 0.283 | 59.971 | 60 | 59.657 | 59.657 | 102.468 |
| $^{14}$C | 0 | 0 | - | 0 | - | - | - | - | 112.496 |
| $^{15}_{\Lambda}$C | 0 | 0 | 0 | 0 | - | - | - | - | 124.962 |
| $^{16}$C | 0.084 | 0.224 | - | 0.296 | 0 | 0 | - | 0 | 118.354 |
| $^{17}_{\Lambda}$C | 0.063 | 0.167 | 0.005 | 0.224 | 0 | 0 | 0 | 0 | 136.242 |
| $^{18}$C | 0.090 | 0.254 | - | 0.342 | 26.078 | 15.290 | - | 17.996 | 124.478 |
| $^{19}_{\Lambda}$C | 0.085 | 0.243 | 0.007 | 0.326 | 25.940 | 15.368 | 19.871 | 18.045 | 138.102 |
| $^{20}$C | 0.083 | 0.234 | - | 0.315 | 47.96 | 11.62 | - | 59.58 | 131.156 |
| $^{21}_{\Lambda}$C | 0.083 | 0.237 | 0.007 | 0.318 | 60 | 59.840 | 60 | 60 | 145.325 |
| $^{22}$C | 0.064 | 0.185 | - | 0.249 | 60 | 59.756 | - | 60 | 132.779 |
| $^{23}_{\Lambda}$C | 0.061 | 0.172 | 0.005 | 0.232 | 60 | 59.770 | 60 | 60 | 147.551 |
| $^{26}$Si | 0.1 | 0.128 | - | 0.224 | 60 | 59.988 | 60 | - | 216.938 |
| $^{27}_{\Lambda}$Si | 0.129 | 0.1 | 0.004 | 0.224 | 60 | 59.900 | 60 | 60 | 233.373 |
| $^{28}$Si | 0.144 | 0.140 | - | 0.278 | 59.979 | 60 | - | 60 | 245.900 |
| $^{29}_{\Lambda}$Si | 0.132 | 0.128 | 0.004 | 0.255 | 59.980 | 60 | 60 | 60 | 262.773 |
| $^{24}$Mg | 0.2 | 0.195 | - | 0.387 | 0 | 0 | - | 0 | 206.924 |
| $^{25}_{\Lambda}$Mg | 0.190 | 0.185 | 0.007 | 0.368 | 0 | 0 | 0 | 0 | 222.714 |
| $^{26}$Mg | 0.104 | 0.126 | - | 0.226 | 59.951 | 60 | - | 60 | 227.144 |
| $^{27}_{\Lambda}$Mg | 0.093 | 0.112 | 0.003 | 0.201 | 59.954 | 60 | 60 | 60 | 243.609 |

per, if we employ the RMF approach instead of the SHF approach. It would be an interesting future subject to carry out three-dimensional calculations for hypernuclei with RMF in order to confirm whether it is the case.

There would be many ways to improve our calculations presented in this paper. Firstly, as the angular momentum projection is shown to be essential to yield the triaxial shape of $^{24}$Mg [42], it may be important to carry out the angular momentum projection on top of the mean-field energy surface in order to discuss the effect of $\Lambda$ particle on the shape of hypernuclei. Secondly, for nuclei with a flat energy surface along the $\gamma$ direction, the generator coordinate method may be required. In particular, it will provide a more quantitative estimate for the energy change of the $\gamma$ vibrational state due to the addition of $\Lambda$ particle. In any case, the mean-field calculations presented in this paper provide a good starting point for these calculations.

It will be an interesting subject to experimentally measure the deformation properties and collective motions of hypernuclei. A discussion has been started for a future experiment of $\gamma$-ray spectroscopy of sd-shell hypernuclei at the new generation experimental facilities, *e.g.,* the J-PARC facility [43, 44]. The change of deformation will be well investigated if excitation energies in a rotational band and the B(E2) values can be measured experimentally.

## Acknowledgments

We thank H. Tamura, Y. Zhang, N. Hinohara and A. Ono for useful discussions. This work was supported by the Japanese Ministry of Education, Culture, Sports, Science and Technology by Grant-in-Aid for Scientific Research under the program number 22540262.

## Appendix A: Overlap between $\Lambda$-particle and nucleon densities

In this Appendix, we discuss the overlap between $\Lambda$ particle and nucleon density distributions using simple parametrizations for the density distributions. Since we consider that a $\Lambda$ particle occupies the lowest single-particle state, we assume that the $\Lambda$ particle density is almost spherical and is given by,

$$\rho_\Lambda(r) = \frac{1}{(\sqrt{\pi}b)^3}\,e^{-r^2/b^2}. \tag{A1}$$

On the other hand, for the nucleon density, we assume that it is given by a deformed Woods-Saxon form, that is,

$$\rho_N(r,\theta,\phi) = \frac{\rho_0}{1+\exp[(r-R(\theta,\phi))/a]}, \tag{A2}$$

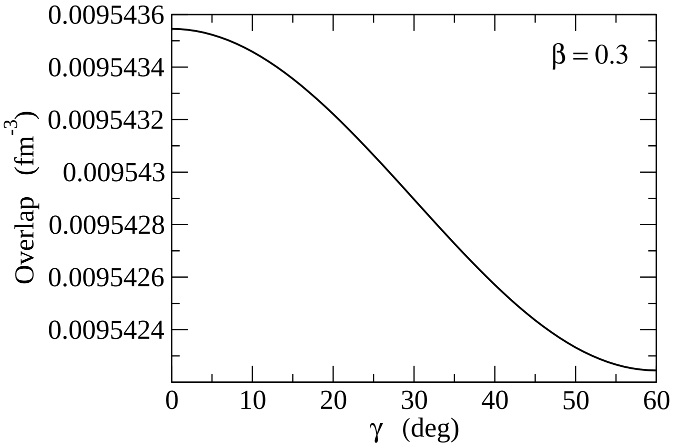

FIG. 14: The overlap between the nucleon and the $\Lambda$ particle densites as a function of the triaxiality $\gamma$ for a fixed value of $\beta = 0.3$. The $\Lambda$-particle density is assumed to be a spherical Gaussian function, while a deformed Woods-Saxon shape is considered for the nucleon density.

where

$$\begin{aligned} R(\theta,\phi) &= R_0(\beta,\gamma)\cdot[1+\beta\cos\gamma\, Y_{20}(\theta) \\ &\quad + \frac{1}{\sqrt{2}}\beta\sin\gamma\,(Y_{22}(\theta,\phi)+Y_{2-2}(\theta,\phi))] \end{aligned} \quad \text{(A3)}$$

Here, the radius $R_0(\beta,\gamma)$ is determined for each $\beta$ and $\gamma$ in order to satifsy the volume conservation condition, that is,

$$F_{\rm vol} = \int_0^\infty r^2 dr \int_{-1}^1 d(\cos\theta) \int_0^{2\pi} d\phi\, \frac{1}{1+\exp([r-R(\theta,\phi))/a]}, \quad \text{(A4)}$$

is independent of $\beta$ and $\gamma$.

Figure 14 shows the overlap between $\rho_\Lambda$ and $\rho_N$, that is,

$$O = \int_0^\infty r^2 dr \int_{-1}^1 d(\cos\theta) \int_0^{2\pi} d\phi\, \rho_\Lambda(r)\rho_N(r,\theta,\phi), \quad \text{(A5)}$$

as a function of the triaxiality $\gamma$ for a fixed value of $\beta = 0.3$. To this end, we use $R_0(\beta=0,\gamma=0) = 1.1\times 24^{1/3}$ fm, and $a$=0.55 fm. The value of $\rho_0$ is fixed so that the volume integral of $\rho_N$ is 24. We use $b$=1.565 fm, which corresponds to the harmonic oscillator with a frequency of $\hbar\omega = 41\times 24^{-1/3}$ MeV. As one can see, the overlap is the largest for the prolate configuration, although the variation is small with respect to $\gamma$.

[1] T. Motoba, H. Bandō and K. Ikeda, Prog. Theor. Phys. **70**, 189 (1983).
[2] E. Hiyama, M. Kamimura, K. Miyazaki, and T. Motoba, Phys. Rev. C**59**, 2351 (1999).
[3] J. Žofka, Czech. J. Phys. **B30**, 95 (1980).
[4] K. Tanida *et al.*, Phys. Rev. Lett.**86**, 1982 (2001).
[5] O. Hashimoto and H. Tamura, Prog. Part. Nucl. Phys. **57**, 564 (2006).
[6] X.R. Zhou, H.-J. Schulze, H. Sagawa, C.X. Wu, and E.G. Zhao, Phys. Rev. C**76**, 034312 (2007).
[7] Myaing Thi Win and K. Hagino, Phys. Rev. C**78**, 054311 (2008).
[8] H.-J. Schulze, M. Thi Win, K. Hagino and H. Sagawa, Prog. Theo. Phys. **123**, 569 (2010).
[9] A. Hayashi, K. Hara and P. Ring, Phys. Rev. Lett. **53**, 337 (1984).
[10] N. Redon *et al.*, Phys. Lett **B181**, 223(1986).
[11] J.A. Sheikh, Y. Sun, and R. Palit, Phys. Lett **B507**, 115 (2001).
[12] P. Bonche, H. Flocard, P.H. Heenen, S.J. Krieger and M.S. Weiss, Nucl. Phys. **A443**, 39 (1985).
[13] M. Girod, J.P. Delaroche, A.Görgen, A. Obertelli, Phys. Lett. **B676**,39 (2009).
[14] Z.P. Li, T. Nikšić, D. Vretenar and J. Meng, Phys. Rev. C**81**, 034316 (2010).
[15] D. Kurath, Phys. Rev. C**5**, 768 (1971).
[16] N. Hinohara and Y. Kanada-En'yo, arXiv:1008.4444v1.
[17] J.M. Yao, H. Mei, H. Chen, J. Meng, P. Ring and D. Vretenar, arXiv:1006.1400.
[18] Y. Zhang, H. Sagawa, D. Yoshino, K. Hagino and J. Meng, Prog. Theo. Phys. **120**, 129 (2008).
[19] D.E. Lanskoy, Phys. Rev. C**58**, 3351 (1998).
[20] T. Harada, Nucl. Phys. **A754**, 86c (2005).
[21] M. Rayet, Ann. of Phys.(N.Y.) **102**, 226 (1976).
[22] M. Rayet, Nucl. Phys. **A367**, 381 (1981).
[23] M. Rufa, H. Stöcker, P.-G. Reinhard, J. Maruhn and W. Greiner, J. Phys. **G13**, L143 (1987).
[24] J. Mares and J. Žofka, Z. Phys. **A333**, 209 (1989).
[25] M. Rufa, J. Schaffner, J. Maruhn, H. Stöcker, W. Greiner and P.-G. Reinhard, Phys. Rev. C**42**, 2469 (1990).
[26] D. Vretenar, W.Pöschl, G.A. Lalazissis, and P. Ring, Phys. Rev. C**57**, R1060 (1998).
[27] X.R. Zhou, A. Polls, H.-J. Schulze, and I. Vidaña, Phys. Rev. C**78**, 054306 (2008).
[28] P. Bonche, H. Flocard, P.H. Heenen, Comp. Phys. Comm.**171**, 49 (2005).
[29] P. Sarriguren, R. Rodríguez-Guzmán, and L.M. Robledo, Phys. Rev. C**77**, 064322 (2008).
[30] N. Tajima, S. Takahara, N. Onishi, Nucl. Phys. **A603**, 23 (1996).
[31] D. Vautherin and D.M. Brink, Phys. Rev. C**5**, 626 (1972).
[32] M. Bender, P.-H. Heenen, and P.-G. Reinhard, Rev. Mod. Phys. **75**, 121 (2003).
[33] J. Terasaki, P.H. Heenen, H. Flocard, and P. Bonche, Nucl. Phys. **A600**, 371 (1996).
[34] Nguyen Van Giai and H. Sagawa, Phys. Lett. **B106**, 379 (1981).
[35] Y. Yamamoto, H. Bandō and J. Žofka, Prog. Theo. Phys. **80**, 757 (1988).
[36] H. Sagawa, X.R. Zhou, X.Z. Zhang and T. Suzuki, Phys.

Rev. C**70**, 054316 (2004).

[37] S.W. Robinson and R.D. Bent, Phys. Rev. **168**, 1266 (1968).

[38] A.V. Cohen and J.A. Cookson, Nucl. Phys. **29**,604 (1962).

[39] R. Batchelor, A.J. Ferguson, H.E. Gove, and A.E. Litherland, Nucl. Phys.**16**, 38 (1960).

[40] W. Koepf and P. Ring, Phys. Lett. **B212**,397 (1988).

[41] P. Bonche, H. Flocard and P.H. Heenen, Nucl. Phys. **A467**, 115 (1987).

[42] J.M. Yao, J. Meng, P. Ring and D. Vretener, Phys. Rev. C**81**, 044311 (2010).

[43] T. Koike, in *Proceedings of the Sendai International Symposium "Strangeness in Nuclear and Hadronic Systems"* (SENDAI08) (World Scientific, Singapore, 2010), p.213.

[44] H. Tamura, Int. J. Mod. Phys. **A24**, 2101 (2009).